J|A|C|S
ARTICLES

On the Origin of Helical Mesostructures

Sui Yang,† Lingzhi Zhao,† Chengzhong Yu,*,† Xufeng Zhou,† Jiawei Tang,†
Pei Yuan,† Daoyong Chen,‡ and Dongyuan Zhao†,‡

Contribution from the Department of Chemistry and Shanghai Key Laboratory of Molecular Catalysis and Innovative Materials, Fudan University, Shanghai 200433, P.R. China, and Department of Polymer Science and Laboratory of Macromolecular Science, Fudan University, Shanghai 200433, P.R. China.

Received March 20, 2006; E-mail: czyu@fudan.edu.cn

Abstract: The investigation on the formation mechanism of helical structures and the synthesis of helical materials is attractive for scientists in different fields. Here we report the synthesis of helical mesoporous materials with chiral channels in the presence of achiral surfactants. More importantly, we suggest a simple and purely interfacial interaction mechanism to explain the spontaneous formation of helical mesostructures. Unlike the proposed model for the formation of helical molecular chains or surpramolecular packing based on the geometrically motivated model or the entropically driven model, the origin of the helical mesostructured materials may be attributed to a morphological transformation accompanied by a reduction in surface free energy. After the helical morphology is formed, the increase in bending energy together with the derivation from a perfect hexagonal mesostructure may limit the curvature of helices. Our model may be general and important in the designed synthesis of helical mesoporous materials.

Introduction

Helical conformation is one of the most fascinating structures in nature. The double-stranded macromolecules of DNA are almost all right-handed helices. The formation mechanisms of this nature-favoring conformation have been explained by the geometrically motivated model[1−4] and the entropically driven model,[5] which do not depend on the molecular chirality such as the residues in the DNA chain. In addition to the helical macromolecular chains, some animals have helical macromorphologies such as horns appearing in both enantiomorphous left- and right-handed forms. Spirals are also found in the shells of snails and of nautilus, a type of marine mollusk. It is not known, however, whether the proposed models[1−5] can be applied to explain the formation of helical macro-morphology in nature.

The fast development of the bio-inspired chemical process in the lab mimicking the natural synthetic routes not only results in materials with amazing composition and morphology at both the micro- and macroscales, [6,7] but also provides scientists with a great chance to go deep into the principles behind. Recently, the synthesis of helical nanostructured materials has become a hot issue.[8−12] Che et al. reported the synthesis of chiral mesoporous materials by using chiral surfactants as templates.[13] Some investigation on external helical morphology in the presence of achiral templates was also reported.[8,10] Such materials are attractive because they might find potential applications in the fields of chiral catalysis and chiral recognition.[13−16] However, the formation mechanism of the chiral channels and the helical morphology is still not known.

In this work, we report the synthesis of helical mesoporous materials by using achiral surfactants. The size and the pitch of the helical rods can be further controlled by the addition of perfluorinated carboxylic acid. More importantly, we present a new interfacial interaction mechanism to explain the formation of mesostructured helical morphology. It is proposed that the reduction in surface free energy is the driving force for the spontaneous formation of the spiral morphology, while the increase in bending energy and symmetry breaking, as results of the formation of the helical mesostructured morphology, may

---

† Department of Chemistry and Shanghai Key Laboratory of Molecular Catalysis and Innovative Materials.

‡ Department of Polymer Science and Laboratory of Macromolecular Science.

(1) Kellogg, G. J.; Walton, D. G.; Mayes, A. M.; Lambooy, P.; Russell, T. P.; Gallagher, P. D.; Satija, S. K. *Phys. Rev. Lett.* **1996**, *76*, 2503−2506.

(2) Lambooy, P.; Russell, T. P.; Kellogg, G. J.; Mayes, A. M.; Gallagher, P. D.; Satija, S. K. *Phys. Rev*. Lett. **1994**, *72*, 2899−2902.

(3) Maritan, A.; Micheletti, C.; Trovato, A.; Banavar, J. R. *Nature* **2000**, *406*, 287−290.

(4) Zhu, S.; Liu, Y.; Rafailovich, M. H.; Sokolov, J.; Gersappe, D.; Winesett, D. A.; Ade, H. *Nature* **1999**, *400*, 49−51.

(5) Snir, Y.; Kamien, R. D. *Science* **2005**, *307*, 1067−1067.

(6) Sanchez, C.; Arribart, H.; Guille, M. M. G. *Nat. Mater.* **2005**, *4*, 277−288.

(7) Soler-illia, G. J. D.; Sanchez, C.; Lebeau, B.; Patarin, J. *Chem. Rev.* **2002**, *102*, 4093−4138.

(8) Yang, S. M.; Sokolov, I.; Coombs, N.; Kresge, C. T.; Ozin, G. A. *Adv. Mater.* **1999**, *11*, 1427−1431.

(9) Wu, Y. Y.; Cheng, G. S.; Katsov, K.; Sides, S. W.; Wang, J. F.; Tang, J.; Fredrickson, G. H.; Moskovits, M.; Stucky, G. D. *Nat. Mater.* **2004**, 3, 816−822.

(10) Yang, S. M.; Kim, W. J. *Adv. Mater.* **2001**, *13*, 1191−1195.

(11) Yang, Y. G.; Suzuki, M.; Owa, S.; Shirai, H.; Hanabusa, K. *Chem. Commun.* **2005**, 4462−4464.

(12) Jung, J. H.; Yoshida, K.; Shimizu, T. *Langmuir* **2002**, *18*, 8724−8727.

(13) Che, S.; Liu, Z.; Ohsuna, T.; Sakamoto, K.; Terasaki, O.; Tatsumi, T. *Nature* **2004**, *429*, 281−284.

(14) Gier, T. E.; Bu, X. H.; Feng, P. Y.; Stucky, G. D. *Nature* **1998**, *395*, 154−157.

(15) Bradshaw, D.; Prior, T. J.; Cussen, E. J.; Claridge, J. B.; Rosseinsky, M. J. *J. Am. Chem. Soc.* **2004**, *126*, 6106−6114.

(16) Yan, X.; Wei, F.; Elangovan, S. P.; Ogura, M.; Okubo, T. *Eur. J. Inorg. Chem.* **2004**, 4547−4549.

10.1021/ja0619049 CCC: $33.50

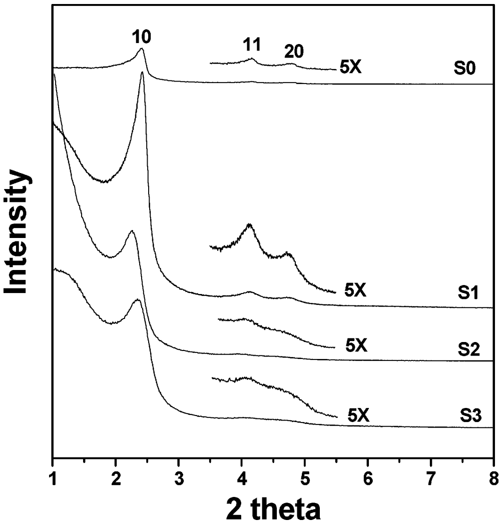

Figure 1. XRD patterns of calcined samples synthesized at different *R*.

compete with the negative surface free energy change. The formation of the chiral channels may be understood as a consequence of homogeneously distributing the bending energy and maintaining a stable hexagonal mesostructure in MCM-41 materials.

Experiment Section

Synthesis. All chemicals were used as received without further purification. Perfluorooctanoic acid (PFOA) was purchased from Aldrich. Other chemicals were purchased from Shanghai Chemical Company. Siliceous helical mesoporous materials with hexagonal structures were synthesized under basic conditions by using PFOA and cetyltrimethylammonium bromide (CTAB) as co-templates with different PFOA/CTAB weight ratios (*R*). In a typical synthesis, 0.20 g of CTAB was dissolved in 96 g of deionized water with stirring at room temperature. Then, 0.70 mL of NaOH (2 M) and a desired amount of PFOA were added separately into the solution. The temperature of the solution was raised and kept at 80 °C. To this solution, 1.34 mL of tetraethyl orthosilicate (TEOS) was added. The mixture was continuously stirred for an additional 2 h. The resulting products were collected by filtration and dried at room temperature. The templates were removed by calcination at 550 °C for 5 h.

Characterization. X-ray diffraction (XRD) patterns of materials were recorded on a German Bruker D4 X-ray diffractometer with Ni-filtered Cu Kα radiation. Transmission electron microscopy (TEM) images were obtained with a JEOL 2011 microscope operated at 200 kV. For TEM measurements, the samples were prepared by dispersing the powder samples in ethanol, after which they were dispersed and dried on carbon film on a Cu grid. Scanning electron microscopy (SEM) images were obtained on a Philip XL30 microscope operated at 20 kV. High-resolution scanning electron microscopy (HRSEM) images were obtained on JEOL JSM-6300F microscope operated at 10 kV. Nitrogen adsorption/desorption isotherms were measured at −196 °C by using a Micromeritics ASAP Tristar 3000 system. The samples were degassed at 180 °C overnight on a vacuum line.

Results and Discussion

Small angle XRD patterns of calcined samples obtained at different *R* are shown in Figure 1. For samples S0, S1, S2, S3 synthesized at $R = 0$, 0.05, 0.075, 0.10, respectively, similar XRD patterns are observed. Three well-resolved peaks in the range of $2\theta = 2-5°$ can be indexed as the 10, 11, and 20 reflections based on a two-dimensional hexagonal symmetry (p6*m*).[17] The *d* spacing calculated from the first diffraction peak is 3.7 nm (cell parameter, *a*, is 4.3 nm), the same for the four samples. In addition, the mean pore size calculated from the nitrogen adsorption branch by the BJH method is 2.6 nm for the above four samples. The physicochemical parameters of S0−S3 are listed in Table 1 for comparison.

Table 1. Silica Samples Prepared from Different PFOA/CTAB Weight Ratio (*R*)[a]

samples	*R*	*d* /nm	*p* /nm	*S* /m^{2}g^{-1}	*V* /mm^{3}g^{-1}
S0	0	3.7	2.6	635	668
S1	0.05	3.7	2.6	616	677
S2	0.075	3.7	2.6	462	592
S3	0.1	3.7	2.6	573	730

[a] *d* is the *d* spacing calculated from the first XRD peak, *p* stands for the pore size calculated from the adsorption branch by BJH method, *S* is the BET surface area, and *V* represents pore volume

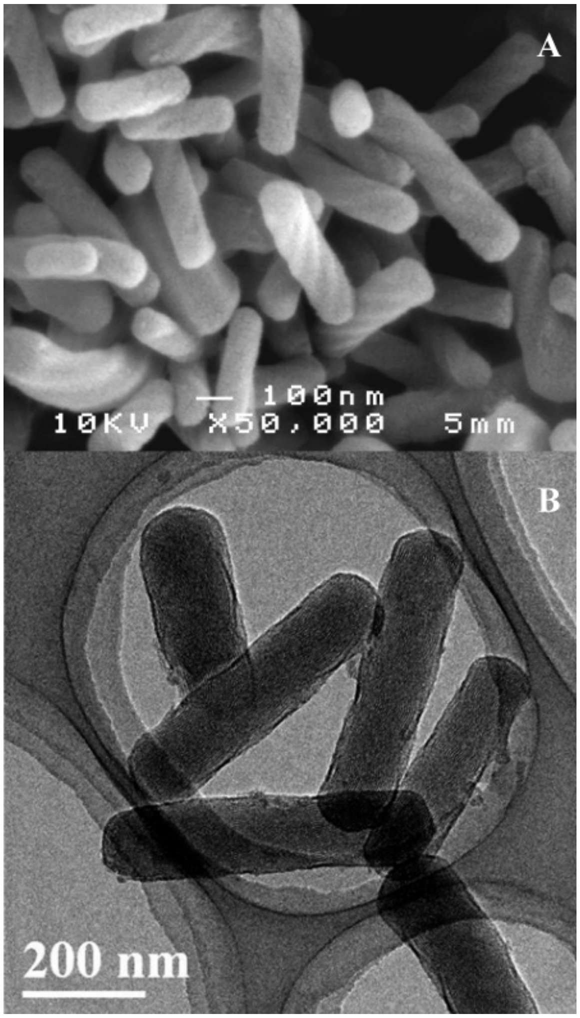

Figure 2. HRSEM image (A) and TEM image (B) of calcined sample S1.

HRSEM image of sample S1 ($R = 0.05$) shows a helical rodlike morphology (Figure 2A). The ratio of right-handed and left-handed helices is 1.1 judged from 110 helical rods obtained in different SEM images. TEM observations of S1 confirm the rodlike morphology (Figure 2B). At high magnifications, the TEM image of S1 represents a periodical appearance of fringes (Figure 3A), indicative of chiral channels within the helical

---

(17) Kresge, C. T.; Leonowicz, M. E.; Roth, W. J.; Vartuli, J. C.; Beck, J. S. *Nature* **1992**, *359*, 710−712.

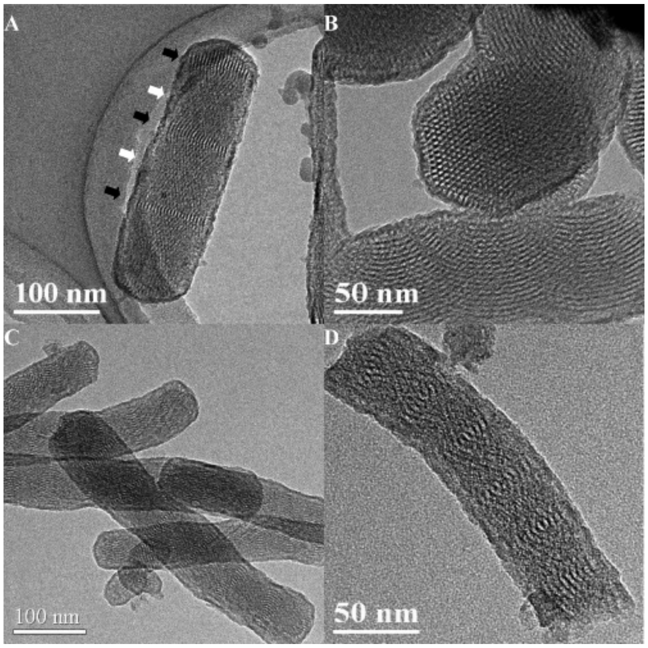

Figure 3. TEM images of calcined samples synthesized with different *R*: (A, B) S1, (C) S2, and (D) S3. The fringes indicated by dark arrows correspond to (10) plane of the hexagonal structure, while the ones indicated by white arrows correspond to (11) plane.

rods.[13,18] It is interesting to note that each helical rod possesses two rounded ends viewing along the direction perpendicular to the rods (Figures 2B and 3A), while the shape of the end (cross section) shows a hexagonal plane (Figure 3B). For the helical rod shown in Figure 3A, the diameter is ~100 nm, and the length is ~320 nm. Along the length of the hexagonally mesostructured helical rods, the clearly recurrent fringes (indicated by dark arrows) correspond to the (10) plane. The narrower, less obvious fringes observed at the center between two neighboring (10) fringes correspond to the (11) plane (indicated by white arrows). The pitch of the helix (*P*), which is 6 times the distance between two sets of the (10) fringes, is calculated to be ~550 nm. In sample S1, the helical mesoporous rods with slightly different diameters and pitch sizes are also observed. The plot of *P* as a function of the diameter (*D*) and length (*L*) of different rods in S1 samples is shown in Figure 4A. The average *P* in S1 samples is 580 ± 100 nm.

For samples S2 and S3 synthesized at $R = 0.075$ and 0.10, respectively, SEM images reveal high yields of rodlike morphologies with smaller sizes compared to images of S1 samples (Figure 5, C and D). However, the structural features cannot be seen under SEM observation due to the smaller particle sizes compared to the size of the particles of S1. TEM images reveal that S2 and S3 are also helical rods with chiral channels along the length of the rods (Figure 3, C and D). The periodic (10) fringes are also observed. Unlike S1 samples in which mostly well-rounded rods are observed, some of the helical rods are broken at one or two ends in S2 samples, while the rods are generally broken at both ends in S3 samples. For this reason, the length of helical rods is not considered in S2 and S3 samples; only the correlation of *D* vs *P* is plotted in Figure 4A for S2 and S3 together with S1 samples. The average *P* in S2 and S3 samples is 360 ± 100 and 210 ± 20 nm, respectively. For helical mesostructured rods (S1−S3), *P* is obviously dependent on the dimension of the rods and decreases as *D* and *L* decrease, and the influence of *D* on *P* is more notable than that of *L* (Figure 4A). More importantly, it is noted that an almost linear *D* vs *P* correlation exists especially when *P* is larger than ~480 nm in S1 samples (Figure 4A).

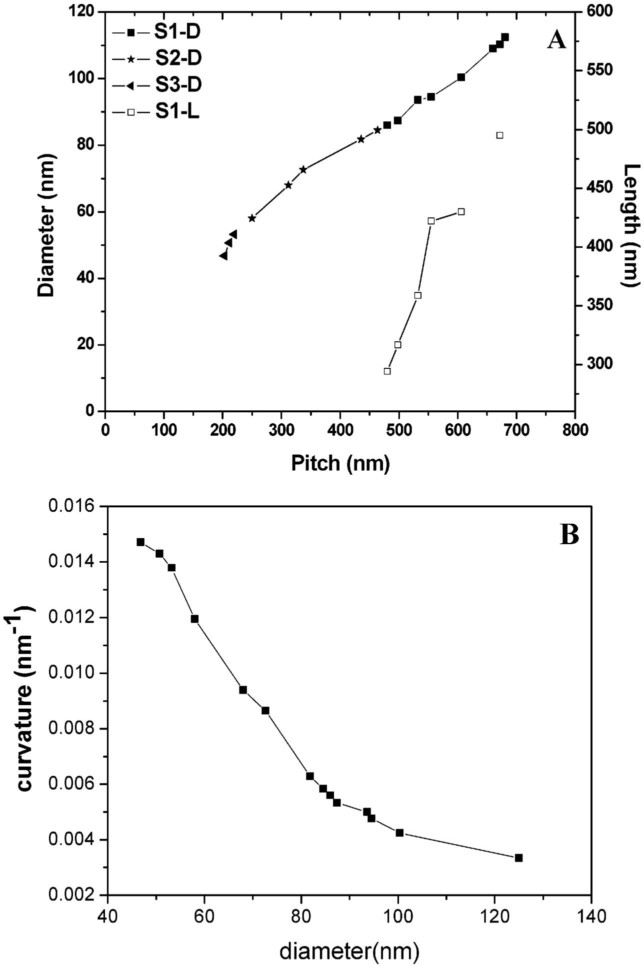

Figure 4. **(**A**)** Plot of diameter (*D*) and length (*L*) versus pitch (*P*). The values were measured from different TEM images. **(**B**)** Relationship between curvature (κ) and diameter (*D*). The values of κ were calculated by the formula $\kappa = r/(r^2 + c^2)$ using the data shown in Figure 4a. Lines between data points are guidance for the eyes.

A helix can be described parametrically by the following equations:

$$\begin{cases} x = r\cos t \\ y = r\sin t \\ h = ct \end{cases} \tag{1}$$

where *r* is the radius, and $c = P/2\pi$. A helix is well defined if its *r* and *P* are specified. In literatures, the pitch-radius ratio (denoted *C*, $C = P/r$) is used to discuss the optimal shapes of closely packed ideal ropes, and the helical conformation with a particular *C* ($C = 2.5$) is selected.[3,5,19] Comparably, in the α helices of commonly found proteins, $C = 2$ is observed as the low bound, in accordance with the simulation results. In contrast, in our samples, *C* is found in a range of 8.4−12, indicating a quite loose helical conformation. The difference in *C* values

---

(18) Ohsuna, T.; Liu, Z.; Che, S. N.; Terasaki, O. *Small* **2005**, 1, 233−237.

(19) Przybyl, S.; Pieranski, P. *Eur. Phys. J. E.* **2001**, *4*, 445−449.

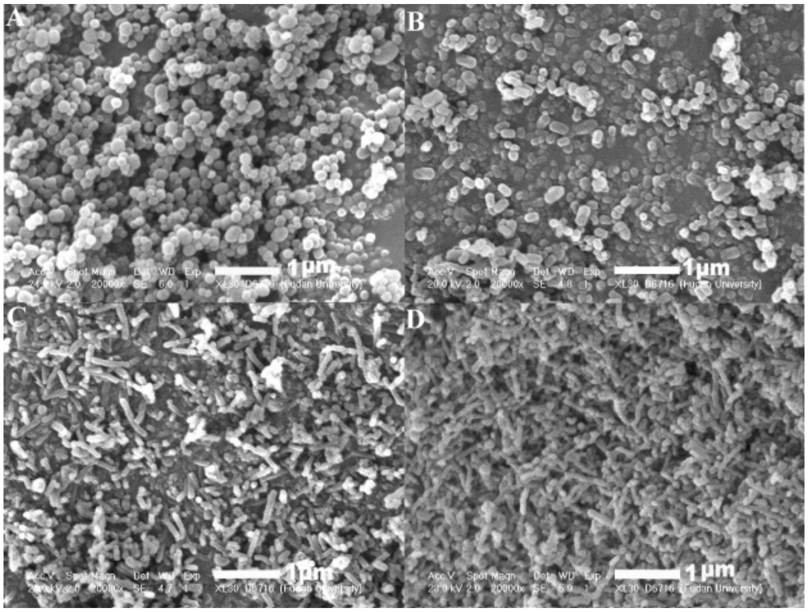

Figure 5. SEM images of calcined samples synthesized with different R: (A) $R = 0$ (S0), (B) $R = 0.025$, (C) $R = 0.075$ (S2) and (D) $R = 0.1$ (S3).

may suggest that the driving forces are different for the formation of helical mesostructured rods (our materials) compared to the helical DNA molecular chains.[5]

Che et al. reported the synthesis of chiral mesoporous materials by using chiral organic molecules as templates.[13] Pleasantly surprised, the chiral mesostructured rods obtained in our approach are assembled from achiral templates. The pitch of helical rods can be adjusted in a certain range by varying R. It is important to consider the formation mechanism of helical hexagonally mesostructured rods in our system. It was reported that the use of fluorinated surfactants together with block copolymers may lead to the formation of highly ordered mesoporous nanoparticles in aqueous solutions[20] and ordered hierarchical mesoporous core−shell nanoparticles by a one-pot aerosol synthesis pathway.[21] We propose that in the range of R under study, the perfluorooctanoate anions with very low surface tension[22,23] may show behaviors similar to those of other fluorocarbon surfactants.[20,21] As a result, it is observed that higher R may lead to smaller particle sizes in S1−S3 samples, while the cell parameter and the pore size of the hexagonal mesostructure is not altered (Table 1). It is important to note that with decreased particle size, the specific surface area of as-synthesized materials (in terms of the particle morphology) increases, and the influence of the surface free energy upon the morphology may become important. In this regard, the origin of the helical mesostructured rods in our system may be attributed to the change in morphology or geometry, rather than other factors such as chiral surfactants or chiral micelles at the molecular scale[24] or the physical confinement at the nanoscale.[9]

Scheme 1. Schematic Drawing Illustrating the Formation of Helical Mesostructured Rods from Hexagonally Arrayed Straight Rodlike Micelles with Equal Length (A) to a Helical Rod with Two Rounded Ends Viewing Perpendicular to the Length Direction (B) and the Hexagonal Cross Section Viewing Parallel to the Length Direction (C)

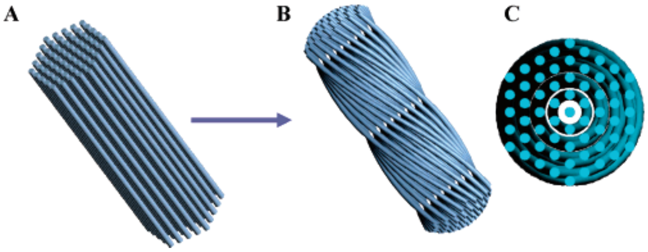

For the helical rods in S1 samples, the shape of the ends (rounded and hexagonal viewed perpendicular and parallel to the length direction, respectively) indicates that the rodlike morphology is a spiral transformed from bundles of hexagonally arrayed and straight rodlike composite micelles with equal length (H) (Scheme 1, Figure 6). The height of a certain helical micelle, h, is measured as the vertical separation of its actual length (arc length) in space. It should be noted that the rodlike micelle right at the center of the helix is straight and has a length of H. The ratio of h versus H can be given by $c/\sqrt{r^2+c^2}$ based on the parametric equation described in the previous paragraph. For the helical rod of S1 sample shown in Figure 6, the shape of the end simulated by mathematic calculations matches well with the observed morphology. Moreover, the theoretical and experimental measured ratio of the height of the most outer micelle h_0 to H is 0.88 and 0.87, respectively, in good accordance with our proposed model.

To understand the spontaneous formation process of helical mesostructures, the morphology, consisting of a bundle of rodlike micelles rather than a single rodlike micelle, should be considered. Although the helical rods show hexagonal cross sections in our materials, we use a cylinder with a circular cross section in the following discussion for simplification. Suppose a spiral cylinder with a radius of r and a pitch size of $2\pi c$ transformed from a straight cylinder with a height of H and a radius of R, assuming that the volume is constant and the length of the helix is equal to H. The surface areas of the straight and spiral cylinder are S and S', respectively. On the basis of the above model, we calculate the S/S' ratio from the helical rods

---

(20) Han, Y.; Ying, J. Y. *Angew. Chem., Int. Ed.* **2005**, *44*, 288−292.
(21) Areva, S.; Boissiere, C.; Grosso, D.; Asakawa, T.; Sanchez, C.; Linden, M. *Chem. Commun.* **2004**, 1630−1631.
(22) Wang, K.; Karlsson, G.; Almgren, M.; Asakawa, T. *J. Phys. Chem. B* **1999**, *103*, 9237−9246.
(23) Thunemann, A. F. *Langmuir* **2000**, *16*, 824−828.
(24) Tracey, A. S.; Zhang, X. *J. Phys. Chem.* **1992**, *96*, 3889−3894.

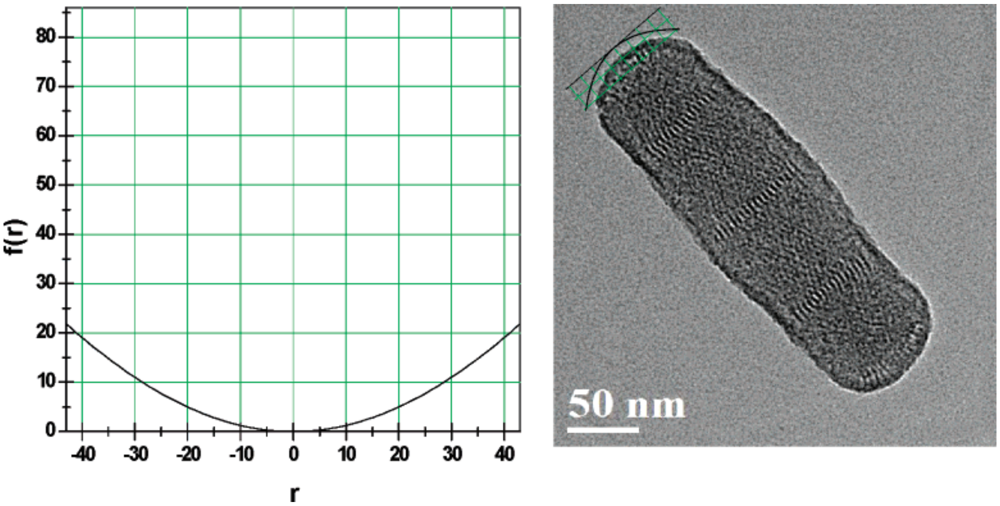

Figure 6. Simulation of the shape of the end of a rodlike S1 sample viewing perpendicular to the length direction (left) and comparison with its TEM image (right). For the simulation, suppose a bundle of straight rodlike micelles with equal length, and then all the rodlike micelles are twisted into helices with a fixed pitch size except that the one right in the middle ($r = 0$) is still straight. For a rodlike micelle located at the position r, its vertical separation is smaller than the actual length in space and the decrement $f(r)$ is a function of $r(f(r) = (\sqrt{r^2+c^2} - c/2c)h)$. For the helical rod shown in the TEM image ($c = 76$ nm, $h = 290$ nm), the curve drawn from the above equation is obtained (left), showing a similar shape to that in the TEM image (right).

Table 2. Surface Area Reduction Calculation Based on Our Proposed Model by Assuming a Geometrical Transformation from a Straight Cylinder to a Spiral Cylinder (see Supporting Information for details)

	samples from TEM image				
parameter[a]	$R = 0.05$				
h /nm	386	440	380	281	384
r /nm	56	55	50	47	47
L /nm	26	30	27	19	18
H /nm	438	500	434	319	420
R /nm	54.4	53.5	48.6	45.7	46
H/R	8.05	9.35	8.93	6.98	9.13
S/S'	1.053	1.053	1.055	1.056	1.042
P /nm	680	672	606	532	535

[a] H and R are the height and radius of the straight cylinder, and the spiral cylinder has a radius of r, a pitch size of $2\pi c$, and a height of h.

observed in TEM images (see Supporting Information for details). The volume and surface area of the ends of the helical rods can be integrated by the equation of the curve (Figure 6). For S1 samples, the transformation from a cylinder to a spiral may lead to an average reduction ratio of surface area of 5.2−6% (Table 2).

On the basis of the above calculations, we suggest a purely interfacial interaction mechanism to explain the formation of mesostructured helical morphology. The reduction in surface free energy (ΔG_S) is the driving force for the spontaneous formation of the spiral morphology. Although the surface area reduction ratio from a cylinder to a helical morphology is not remarkable (5−6% observed), the reduction of surface free energy is related not only to the ratio but also to the specific surface area and the specific surface free energy of materials. In this regard, decreasing the particle size may increase the specific surface area and therefore further decrease the surface free energy, favoring the spontaneous formation of helical morphologies. It is noted that, in a range of helical rods in S1 samples with different H, D, and P, a similar specific surface area reduction is observed, indicating a constant surface free energy reduction (assuming a constant specific surface free energy).

Although the formation of the spiral morphology is a spontaneous process in view of the negative ΔG_S, however, increasing the extent of the helix may lead to the derivation from a perfect hexagonal symmetry and a relatively less stable mesostructure. This may be understood by introducing the curvature (κ) of a helix where $\kappa = r/(r^2 + c^2)$. Obviously, κ of one individual rodlike micelle in the helical mesostructured rod depends on P and r. The curvature of the inside rodlike micelle decreases with decreased r, approaching zero in the center. Therefore, the assembly of rodlike micelles with different κ may break the hexagonal symmetry to a certain degree. Moreover, the transformation from a straight rodlike micelle to a helical one is accompanied by an increase in bending energy (ΔG_B).[25] The positive ΔG_B as well as the symmetry breaking as results of the formation of the helical mesostructured rodlike morphology is energetically unfavorable; their competition with ΔG_S may prevent the formation of more curved helical morphology.

It is noted that the formation of the chiral channels in MCM-41 material is a consequence of the helical morphology and is closely related to its hexagonal mesostructure. The transformation from a straight one-dimensional rodlike composite micelle to a helical one is more favorable than other possible conformations because κ of one helix is a constant at any point in space; thus, the bending energy can be homogeneously distributed within one individual rodlike composite micelle, and the derivation from a perfect hexagonal mesostructure can be minimized.

We selectively calculated κ of the rodlike micelle at the edge of the helical rods in S1−S3 samples. The plot of κ as a function of D is shown in Figure 4B. For helical rods with smaller D, κ of the most outer rodlike micelle is larger. Since ΔG_B is proportional to κ^2 in S1−S3 samples, the ΔG_B of the most outer rodlike micelle in helical rods with smaller D is also higher than that with larger D. When κ increases to a certain value, the ordered hexagonal liquid crystal phase may be not stable. This is also confirmed in our experiments when $R > 0.1$ (data not shown).

---

[25] Ricca, R. L. *J. Phys. A: Math. Gen.* **1995**, *28*, 2335−2352.

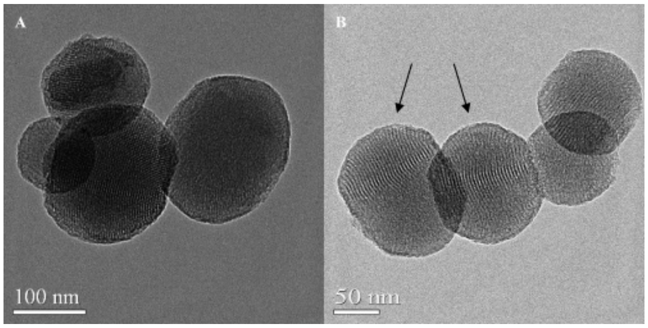

Figure 7. TEM images of a calcined sample synthesized at $R = 0$ (S0).

It should be mentioned that our model may be applied with the condition that the length of the hexagonal morphology is larger than the diameter ($H > D$). For a cylinder with a constant volume, the minimum surface area is achieved when $H = D$. In other words, for a cylinder with $H > D$, a morphology transformation to a spiral may be energetically favorable to reduce the surface free energy, although the ratio of surface area reduction is quite small when H approaches D. In contrast, for a cylinder with $H \leq D$, the transformation to a helical shape cannot take place spontaneously because this process comes with an increase in surface area.

At a first glance, the above simple mechanism is quite surprising and abnormal because one may infer that the preferred helical morphology ($H > D$) should have been observed in normal MCM-41 materials.[17] To answer this question, sample S0 synthesized in the absence of PFOA was investigated. Both SEM (Figure 5A) and TEM observations (Figure 7A) reveal a near spherical morphology. The hexagonal mesostructural regularity of S0 is less ordered compared to that of S1 samples, which is also reflected by the relatively lower intensity of XRD peaks (Figure 1). The formation of a near spherical morphology with less ordered hexagonal mesostructure is not surprising, which can also be attributed to the interfacial interaction to minimize surface area. A few samples indicated by arrows show a short cylindrical shape and one (10) fringe (Figure 7B). The pitch size cannot be determined in such particles. To make it more clear, a sample synthesized at $R = 0.025$ was further investigated (Figure 5B). One helical rod ($D = 110$ nm, $H = 200$ nm) shows two clear (10) fringes and one less obvious (11) fringes (Figure 8). The pitch size is estimated to be >800 nm. The above facts suggestthat the formation of helical mesostructures is not dependent on the use of PFOA co-templates. Nevertheless, by comparing S1 with S0 samples, the use of PFOA may lead to the formation of a more ordered hexagonal rodlike morphology with larger aspect ratio ($H > D$), favoring the formation of helical mesostructured morphology. Of course, the true role of PFOA should be further studied, and the interaction of the perfluorooctanoate anions with CTA cations in our system should also be taken into account, especially at high R ratios. Finally, by just looking at S0 itself, one would not give this assignment (helical conformation) if S0 were studied individually rather than observed systematically in the present study.

We also use Cryo-TEM to investigate the helical structure formation process in solution. No evidence of chiral rodlike micelles in solution is observed. This is not surprising; otherwise, it would be difficult to understand that helical rodlike micelles with the same pitch but different curvature may selectively self-assemble together (remember for $R = 0.050$ samples, helical rods with different P are observed). At the time of precipitation, disordered rodlike morphology was observed. Only after 1 min of precipitation were observed the helical rods with well-ordered fringes (Figure 9). We propose that the helical morphology and the hexagonally chiral mesochannels are most likely generated simultaneously in solution.

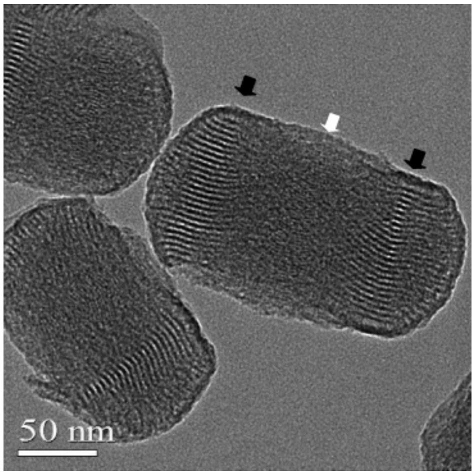

Figure 8. TEM image of a calcined sample synthesized at $R = 0.025$

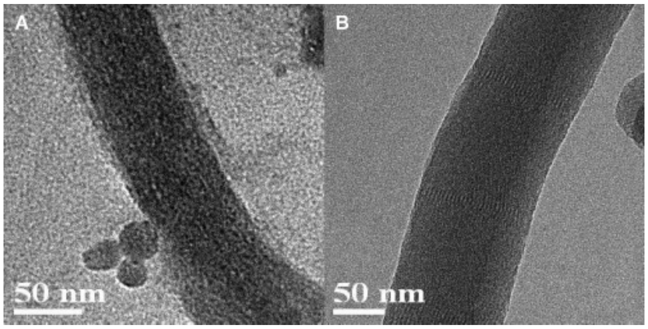

Figure 9. Cryo-TEM of sample S1: (A) as soon as precipitation occurred in solution; and (B) 1 min after precipitation.

On the basis of our proposed interfacial interaction model, we predict that the helical morphology may be formed when ΔG_S is greatly reduced. In this regard, forming a rodlike morphology ($H > D$), decreasing the particle size (increasing the surface area), and decreasing the specific surface free energy are all energetically favorable. On the contrary, factors that increase the ΔG_B (such as increasing the stiffness of composite rodlike micelles) may be disadvantageous for the formation of helical morphology. Moreover, our model is not limited to hexagonally mesostructured materials. It is anticipated that mesoporous materials with helical morphology and different mesostructure may also be prepared. The current mechanism may also be applied to explain the origin of other helical morphologies observed in nature.

Conclusions

Helical mesoporous materials with tunable pitch size have been synthesized in the presence of achiral surfactants. Most importantly, we suggest a purely interfacial interaction mechanism to explain the formation of helical mesostructures. With this model, the reduction in surface free energy is the driving force for the spontaneous formation of the spiral morphology, while the increase of bending energy and the derivation from a perfect hexagonal mesostructure after the helical morphology is formed may limit the curvature of the helices. Our proposed model may be applied to explain the formation of other helical morphologies and important in the designed synthesis of new materials.

Acknowledgment. This work is supported by the National Science Foundations of China (20301004, 20573021, 20421303, and 20233030), the State Key Research Program (2004CB217800), the Shanghai Science Committee (03QF14002), and FANEDD (200423).

Supporting Information Available: The calculation process of surface area reduction based on our proposed model. This material is available free of charge via the Internet at http://pubs.acr.org.

JA0619049